SSRG International Journal of Civil Engineering
ISSN: 2348-8352/ https://doi.org/10.14445/23488352/IJCE-V12I4P117

Volume 12 Issue 4, 181-193, April 2025

Original Article

Experimental Study on the Production of One-Part Alkali-Activated Foam Mortar Containing Eggshell Waste

Kübra Ekiz Barış

[1]*Department of Architecture and Design, Kocaeli University, Kocaeli, Türkiye.*

[1]*Corresponding Author : kubra.ekizbaris@kocaeli.edu.tr*

Received: 12 February 2025 Revised: 14 March 2025 Accepted: 15 April 2025 Published: 30 April 2025

Abstract *- Eggshell (ES) is an agro-based waste that produces alkali-activated materials. Although most of the research is focused on ES-based Alkali-Activated Mortars (AAM), Alkali-Activated Foam Mortars (AAFM) production is quite scarce. Using caustic aqueous alkaline solutions in traditional two-part mixing methods results in substantial dangers during large-scale applications. This study presents an opportunity to produce one-part AAFM, foamed with aluminum powder (Al), that uses metakaolin (MK) and ES as aluminosilicate precursors. The impacts of MK:ES and Al contents on the properties are researched. The highest density (D) (1.81 g/cm^3), ultrasound velocity (UV) (2.33 km/s), Compressive Strength (CS) (12.50 MPa), and the lowest porosity (P) (15.35%), water absorption ratio (WAR) (9.82%), and Drying Shrinkage (DS) (511 µs), are detected in the samples with 70% of MK and 30% of ES. The pore size distributions change with Al content. Gradually increasing Al content to 1.50% results in an increase in the volume of macropores. The lowest thermal conductivity coefficient (TC), 0.187 W/mK, is determined in the (70MK:30ES)-1.50%Al sample. One-part AAFMs with various Al contents may be used as non-loadbearing wall materials, such as lightweight aggregate concrete, pumice concrete, aerated autoclaved concrete, and lightweight bricks.*

Keywords *- Alkali activation, Eggshell waste, Foam mortar, One-part mixing method, Wall material.*

1. Introduction

AAFM is a lightweight mortar with closed air voids contained within its matrix using various foaming techniques. AAFM can be produced either by mixing the mortar with pre-produced foams or by adding a chemical foaming agent (Al or H_2O_2) to the mortar mixture, which generates gas through reactivity with the liquid matrix [1]. During this gas release, voids form in the mortar, resulting in an increase in P and a decrease in D and TC. The addition of 0.5-1.5 wt.% of foaming agent in the AAMs could decrease the TC by 66% in comparison to the reference mortar.

The D and TC of AAFMs and foamed concretes are generally 16-70% and 8-19% lower than those of conventional mortars and concretes [2]. Therefore, AAFM offers several benefits in construction, including lowering the structure's dead load and improving the thermal and acoustic efficiency of building envelopes due to its porous internal structure [3].

Due to these distinctive properties, AAFMs can be used for various nonstructural architectural and civil engineering applications, such as cavity filling, thermal and acoustic insulation, soil stabilization, and the production of lightweight blocks or panels. Furthermore, AAFMs are more sustainable than traditional OPC-based foams and could achieve up to 80% energy savings [4].

An experimental study concluded that the addition of 0.5-1.5 wt.% H_2O_2 decreased the TC of the MK and bagasse ash-based AAFM by 66% compared to the reference sample without a foaming agent [3]. In another study, fly ash (FA)-based AAFM with 74-81% of P, 0.07-0.09 W/mK of TC, and 0.4-1.4 MPa of CS were produced using 0.05-0.1 wt.% H_2O_2 [5]. Other researchers stated that FA-based H_2O_2-containing AAFMs exhibited 0.32-0.98 g/cm^3 D and 0.084-0.175 W/mK TC, while Al-containing AAFMs had 0.51-0.78 g/cm^3 D and 0.098-0.158 W/mK TC [6].

According to another study's results, FA-based, sodium perborate-containing AAFMs had 0.64-0.82 g/cm^3 D, 0.27-0.33 W/mK TC, and 4.3-4.9 MPa CS [7]. Incorporating the silica fume (SF) blowing agent also increased the P up to 65-85% and decreased the TC to between 0.12 and 0.33 W/mK in the MK-based AAFMs [8]. In another study, H_2O_2-included MK-based AAFMs had 0.35-1.20 g/cm^3 D, 0.13-0.32 W/mK TC, and 0.4-5.65 MPa CS [9]. Al incorporation (3-12 wt.%) in the MK-based mortar improved the thermal insulation ability of the material with the highest P of 70% and the lowest TC of 0.15 W/mK [10].

Apart from FA and MK, there are experimental studies that also use various waste materials in AAFM production to increase sustainability. Sawdust (SD)-based materials foamed with H_2O_2 had 0.112-0.125 W/mK TC and 0.76-1.71 MPa CS [11]. Al-containing glass powder-based material exhibited 0.23-0.55 g/cm^3 D, 0.065-0.186 W/mK TC, and 3.0 MPa CS [12]. In another research, 71.9% P and 0.169 W/mK TC were achieved in the red mud/slag-based H_2O_2-containing foams [13].

ES, the outer layer of an egg, is an agro-based waste and can also be utilized to produce cement-based or alkali-activated-based materials. According to the global egg production reports [14], 86.7 million tons of eggs were produced globally in 2020. Figure 1 represents ten countries that stand out in global egg production. Over one-third of the world's egg production comes from China, followed by the United States and India [14]. Türkiye has a share of 2% in global egg production and ranks ninth. ES comprises approximately 10% of the egg weight [15]. Therefore, more than 8 million tons of ES waste are generated worldwide each year [16].

This waste is dumped into landfills, which leads to environmental pollutants and creates allergies. In addition, the scarcity of natural lands due to rapid urbanization leads to an increase in the cost of landfills [17]. In order to divert the maximum amount of ES waste from landfills, it should be used as a raw material in the building industry [18].

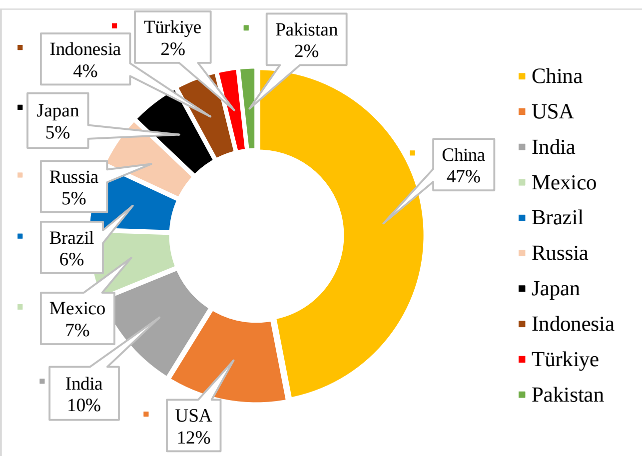

Fig. 1 The main global egg-producing countries [13]

ES has a high calcium content in the chemical form of calcium carbonate, similar to limestone [19]. Therefore, ES wastes can be an alternative to limestone in cement production or may be utilized as a replacement for any kind of material [20]. ES can be used as a raw material for mortar, concrete, fibre-reinforced concrete, masonry block, and as a stabilizer for soil and fired clay-based bricks or blocks [16]. ES may also be used as a raw material in AAMs. Shekhawat et al. [18, 21] researched the mechanical properties of ES and FA-based AAM to find the optimum mixing ratios. Mixtures with 50% ES and 50% FA were found to be optimal for CS. In another study [22], it was found that a 50% ES and 50% FA mixture filled the pores between soil particles and improved the properties of the matrix, which was in line with the findings of Anburuvel et al. [23].

In another research, Mashri et al. [24] produced AAM by using palm oil fuel ash (POFA), eggshell ash (ESA), and SF. The samples with an optimum mixing ratio of POFA (77%), ESA (11.5%), and SF (11.5%) had a CS of 125.4 MPa after 28 days. Omur et al. [25] stated that incorporating ES up to 40% in MK-based AAM increased the CS by 46%. Yuan et al. [26] concluded that ES could improve the strength of FA-based alkali-activated concrete.

Although most of the research is focused on producing AAMs containing ES waste, research on the production of ES-based AAFM is quite scarce in the literature. Only in a study did Abdellatief et al. [2] use SD and ES to produce GGBS+FA-based AAFM, which was foamed with Al. The results revealed that the optimum SD and ES ratios were 5 and 10 wt.%, respectively. 0.3-1.50 wt.% Al-containing samples exhibited 1.79-1.92 g/cm^3 D, 1.167-1.237 W/mK TC, and 9.37-17.45 MPa CS. However, in the study of Abdellatief et al. [2], the alkaline activators were added to the mortar by the traditional two-part alkali-activation method (as solutions).

The two-part method produces caustic, sticky, and extremely concentrated aqueous alkaline solutions. This results in substantial dangers and difficulties working with large-scale and cast-in-place applications. Although the one-part technique has not yet been commercialized in comparison to its conventional two-part counterpart, future investigations will enable the widespread usage of one-part AAMs. Thus, in the last few years, the one-part method has drawn a lot of attention from the academic and industrial sectors because, in contrast to the two-part technique, it offers safer and easier handling for site applications [28, 29].

According to the literature analysis, although recent studies have focused on foam-based materials such as foamed mortars and concretes, investigation into producing lightweight, environmentally friendly construction materials is still needed. Furthermore, there is also a significant gap in the literature regarding the production of ES-based AAFM using the one-part method. Therefore, the current study presents an opportunity to produce a novel one-part AAFM that focuses on the potential use of ES waste.

The novelty of this research is evaluating ES waste in producing a sustainable lightweight AAFM for the construction sector by applying an innovative one-part production method. The physical, mechanical, and thermal characteristics of the AAFM were examined using a comprehensive experimental methodology.

2. Materials and Methods

2.1. Raw Materials

MK and ES were used as aluminosilicate precursors in the AAFM synthesis. MK was obtained from the Kaolin Company, and ES was supplied by the local bakeries in Kocaeli, in Türkiye. MK was prepared for use by drying in a ventilated oven at 100 ºC. The collected ESs were washed thoroughly to eliminate the contaminants and the organic layer. Afterwards, ES was dried under natural sunlight. The ES was then crushed into small pieces, pulverized using a laboratory-type grinder, and passed through a 90 µm sieve. The particle size distributions of the raw materials are shown in Figure 2, revealing that MK has finer particles compared to ES. While 76.0% of ES passes through the 45 µm sieve, 99.3% of MK also does.

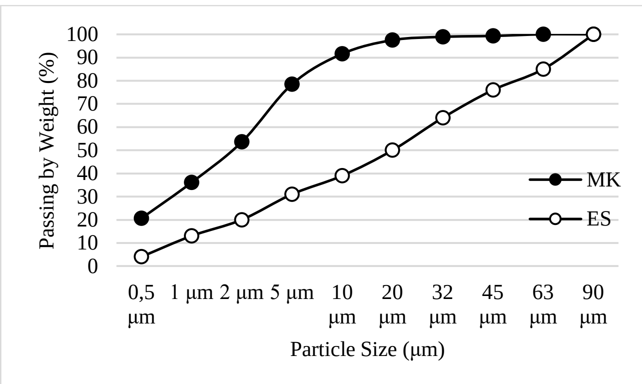

Fig. 2 Particle size distributions of the aluminosilicate precursors

The specific gravities of the MK and ES were determined as 2.34 and 2.31, respectively. The chemical compositions of both raw materials, including their major constituents, are presented in Figure 3.

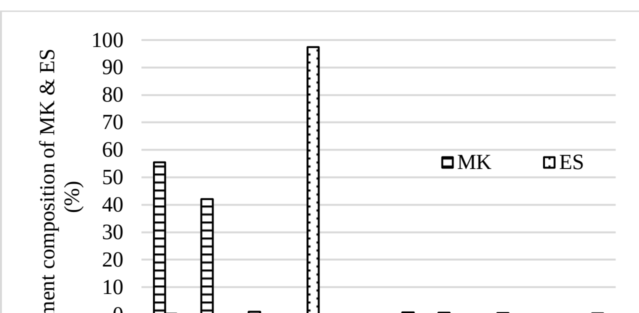

	SiO2	Al2O3	Fe2O3	CaO	TiO2	MgO	K2O	Na2O	SO3	P2O5
MK	55.50	42.04	1.00	0.11	0.23	0.15	0.66	0.10	0.00	0.00
ES	0.39	0.00	0.00	97.49	0.00	0.85	0.00	0.59	0.22	0.46

Fig. 3 Chemical compositions of the aluminosilicate precursors

MK has significant SiO_2 (55.50%), Al_2O_3 (42.04%), and Fe_2O_3 (0.70%) contents, meaning that MK is a pozzolanic material. This pozzolanic activity of the MK was tested according to the TS 25 [29]. Flexural and CS results (2.23 MPa and 19.11 MPa, respectively) revealed that MK, with high pozzolanic character, fulfils the requirements of TS 25. ES mainly comprises CaO (97.49%) and contains a very small amount of SiO_2+Al_2O_3+Fe_2O_3 (0.39%). Its total alkali content (Na_2O+K_2O) is 0.59%. Therefore, the ES may be assumed to be a natural carbonate-based raw material [30].

The outermost layer of ES consists of calcium carbonate, and its composition is comparable to calcitic limestone [30]. The XRD of the MK and ES is given in Figure 4. Calcite, a form of calcium carbonate ($CaCO_3$), was determined in the XRD pattern of ES, whereas the quartz and mica peaks were identified in the XRD pattern of MK. The amorphous phase of MK was determined to be 86%.

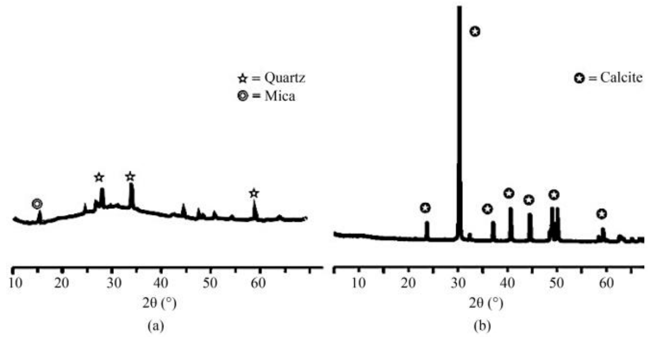

Fig. 4 The XRD of the aluminosilicate precursors: (a) MK, (b) ES

Finely crushed silica sand (SS) having a specific gravity of 2.61 and a maximum particle size of 200 µm was supplied from Ytong Industry in Türkiye and was used as aggregate for the production of AAFM. Al, with 99% purity and a particle size of 50 µm, was supplied from Ytong Industry and used as a foaming agent. In order to initiate the alkaline activation reactions, an industrial-level solid NaOH with 98% purity and anhydrous sodium metasilicate (Na_2SiO_3) (SMS) consisting of 50-52% SiO_2 and 50-48% Na_2O contents were used as chemical alkali activators.

2.2. Mixture Proportions

The experimental stage of the current study consists of two consecutive phases. In the first stage, the impact of MK:ES content on the properties of the AAM was researched. The MK was replaced by ES in proportions of 10-40% by weight. After the optimum MK:ES content was determined, in the second stage, the impact of Al content on the physical, mechanical, and thermal properties of AAFM was investigated. Al was incorporated in the mixtures with 0.25, 0.50, 1.00, and 1.50% by weight of the total precursor, consisting of MK and ES.

The sample produced from 100% MK (without ES and Al) was defined as the reference sample. The total alkali activator: aluminosilicate precursor, the NaOH: SMS, and the binder: SS ratios remained constant at 1:5, 1:2, and 1:2, by weight, respectively. A constant water-to-binder ratio of 0.40 was chosen. All of these mixing ratios, defined as "constant", were the optimum values obtained from the preliminary experiments. The specific mixing ratios required for the production of 3 samples having 40x40x160 mm in size are given in Table 1.

The produced samples were coded in the format [(xMK:yES)-a%Al]. In this coding, "x" and "y" symbolized the contents of MK and ES, respectively. "a%" symbolized the Al content by weight of the total precursor (MK+ES).

Table 1. Mixture proportions of the produced samples

Stage	Sample	MK (g)	ES (g)	SS (g)	Al (g)	NaOH (g)	SMS (g)	Al content (wt.%)	Activator: precursor (wt.%)
I	(100MK)-0%Al	400	-	800	-	33.6	66.6	-	1:5
	(90MK:10ES)-0%Al	360	40						
	(85MK:15ES)-0%Al	340	60						
	(80MK:20ES)-0%Al	320	80						
	(75MK:25ES)-0%Al	300	100						
	(70MK:30ES)-0%Al	280	120						
	(65MK:35ES)-0%Al	260	140						
	(60MK:40ES)-0%Al	240	160						
II	(70MK:30ES)-0.25%Al	280	120		1			0.25	
	(70MK:30ES)-0.50%Al				2			0.50	
	(70MK:30ES)-1.00%Al				4			1.00	
	(70MK:30ES)-1.50%Al				6			1.50	

2.3. Sample Production and Curing Conditions

To synthesise each formula, dry raw materials were mixed manually in a bowl for 2 minutes. Afterwards, with the addition of water, the mixture was mixed using a mixer for 3 minutes. The wet mixture was poured into 40×40×160 mm prismatic moulds. In samples containing Al, heat release and bubble formation started within a short time after moulding. The reaction of Al with aqueous solutions of NaOH is given in Equation (1) [31]. The hydrogen gas bubbles generated according to this equation led to the expansion of the AAM. The volume expansion period of the AAFM was approximately 10-12 minutes. Afterwards, the moulds were sealed and cured in a ventilated oven at 80 °C for 24 h. After heat curing was completed, the samples were left to ambient curing at 21±2 °C and 50±5% RH for 28 days.

$$2Al + 6H_2O + 2NaOH \rightarrow 2NaAl(OH)_4 + 3H_2 \quad (1)$$

2.4. Experimental Methods

The physical tests, such as D, WAR, P, and DS, and the mechanical tests, including UV and CS, were applied to three prismatic samples 40×40×160 mm in size. The mercury intrusion porosimetry (MIP) test was conducted using three 10 x 10 x 10 mm samples, and the TC test was conducted using six samples with a circular cross-section measuring 100 mm in diameter and 10 mm in thickness. The weights of the samples in dry and water-saturated situations, as well as those suspended in water, were measured in order to ascertain D, WAR, and P values. The samples were dried in an oven at 100 °C until they attained a consistent weight, which took around 36 hours, in order to determine the dry sample weight (m_d). To find the water-saturated weight (m_s), the same samples were then stored for 48 hours in a container filled with water. The weight in water (m_h) is the weight of the samples suspended in a container filled with water. Equation (2) was used to figure out the D (ρ, g/cm^3) in compliance with TS EN 1015-10 [32]:

$$\rho = \frac{m_d}{m_s - m_h} \quad (2)$$

In compliance with TS EN 13755 [33], the WAR (%) of the samples at atmospheric pressure was determined using Equation (3):

$$WAR = \frac{m_s - m_h}{m_d} \times 100 \quad (3)$$

The specific weight (the weight of the material without pores) needs to be determined to calculate the P. A specified quantity of material is finely ground into powder form, added to a glass container filled with water, and allowed to settle entirely at the bottom without any air bubbles. This is done in order to calculate the specific weight (ρ_r, g/cm^3) in accordance with TS 699 [34]. Equation (4) was used to get the specific weight:

$$\rho_r = \frac{m_{kn} - m_k}{(m_{kn} - m_k) - (m_{kns} - m_{sd})} \quad (4)$$

The weight of the empty glass container is represented by the character "m_k," the weight of the container filled with the sample by the character "m_{kn}," the weight of the container filled solely with water by the character "m_{sd}," and the weight of the container filled with both water and the sample by the character "m_{kns}." Equation (5) was used to determine the P, (%):

$$P = \left[1 - \left(\frac{\rho}{\rho_r}\right)\right] \times 100 \quad (5)$$

The MIP test was applied to characterize pore volume and pore size distributions of the AAFM using the AutoPore IV 9500 (Micromeritics) porosimeter, covering pore diameters from 0.005 µm up to 500 µm. The surface tension was 485 dynes/cm, and the contact angle was 130°, respectively.

DS was tested for a 90-day curing period in accordance with TS EN 1920-8 [35]. After demoulding, the DS of each sample was calculated on each of the following days (1, 2, 3, 4, 5, 6, 7, 15, 22, 30, 40, 50, 60, 70, 80, and 90), according to Equation (6):

$$DS = \frac{\varepsilon_f - \varepsilon_i}{\varepsilon_i} \qquad (6)$$

"ε_f" and "ε_i" were the final and initial lengths of the sample.

Under compliance with ASTM C518-17 [36], the TC was measured under steady-state circumstances using a heat flux measurement apparatus. The samples were placed between the plates, and the heat flow was monitored. Heat flux (Q, W/m^2) and temperature differentials between the copper plates ($\Delta T = T_1 - T_2$) were measured using the sensors. Equation (7) was used to get the TC (λ, W/mK):

$$Q = \lambda \times \frac{\Delta T}{d} \qquad (7)$$

"d" was the thickness of the sample in m.

A Proceq instrument was used to measure the UV in compliance with TS EN 14579 [37]. By placing probes at both ends of the samples, the instrument automatically determines the UV. Equation (8) was utilised to determine the UV (km/s):

$$UV = \frac{L}{t} \qquad (8)$$

"L" was the length of the sample in mm, and "t" was the time until the sound wave provided by the transmitting probe was received by the receiving probe in µs.

The CS test was applied in accordance with TS EN 196-1 [38] using UTEST 2000 kN (50 N/s) equipment. The CS (MPa) was determined using Equation (9):

$$C_s = \frac{F_c}{A} \qquad (9)$$

"F_c" is the maximum load the sample receives in N; "A" is the area of the cross-section of the sample in mm^2.

3. Results and Discussion

3.1. The Impact of MK:ES Content on the Mechanical Properties of the AAM

Figure 5 shows the influence of MK:ES content on the mechanical properties of AAM samples.

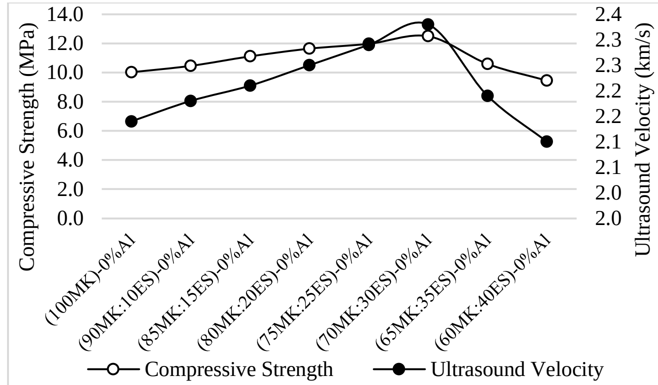

Fig. 5 The impact of MK:ES content on the mechanical properties of AAM

Regardless of the mix proportions, the UV of the samples ranged between 2.10 km/s and 2.33 km/s, and the CS ranged between 9.46 MPa and 12.50 MPa at 28 days. The UV and CS values of the reference sample (100MK-0%Al) were 2.14 km/s and 10.03 MPa, respectively. ES incorporation of up to 30% increased the UC and CS by 8.9% and 24.6%, respectively, compared to the reference mixture. The highest mechanical properties (2.33 km/s UC and 12.50 MPa CS) were detected in the (70MK:30ES)-0%Al sample. The combination of MK and ES contributed to the beneficial role of ES (up to 30%) in enhancing the mechanical properties. Sodium alumina silicate hydrate gel (NASH), which was comparable to those that had been described in the literature [39, 40], was the primary reaction product of the reference sample. The incorporation of ES might accelerate the reactions by forming calcium aluminosilicate hydrate gel (CASH) along with NASH because of its high CaO concentration (97.49% of CaO). These gels worked together to provide a denser microstructure and played an important role in improved mechanical characteristics [18, 25, 41]. Another parameter that contributes to the development of the properties of the MK-based AAM was the micro aggregate effect of ES within the matrix [42]. The unreacted ES components, consisting of $CaCO_3$, could function as micro-aggregates and result in an increase in the mechanical properties. The mechanical properties gradually decreased beyond this optimum ES ratio (>30%). The main reason for this result might be decreasing amounts of dissolved alumina and silica components in the mixtures rich in ES and, consequently, insufficient NASH gel formation in the matrix. The lowest mechanical properties (2.10 km/s UC and 9.46 MPa CS, respectively) were detected in the sample richest in ES (60MK:40ES)-0%Al.

The CS values (9.46-12.50 MPa) determined in the current research are similar to the CS values obtained in other AAM-based studies containing ES. For instance, Omur et al. [25] concluded that the CS of MK-based AAMs with various ES contents (from 20% up to 80%) were approximately between 5 MPa and 62 MPa after 28 days. Shekhawat et al.

[18] determined that the highest CS of FA-based AAMs was 2.1 MPa in the mixture consisting of 50% FA and 50% ES at 56 days. Feng et al. [43] determined that CS of FA-based AAMs with different ES contents (up to 20%) were between 12.4 MPa and 33.9 MPa, according to changes in ES content, activator ratio, liquid-to-solid ratio, and alkaline hydroxide concentration.

3.2. The Impact of MK:ES Content on the Physical Properties of the AAM

Figure 6 illustrates the influence of MK:ES content on the physical properties of AAM samples.

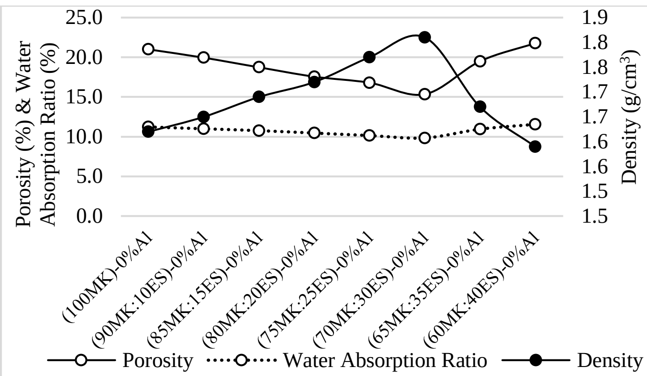

Fig. 6 The impact of MK:ES content on the physical properties of AAM

Regardless of the mix proportions, the P, D, and WAR of the samples ranged between 15.35% and 21.78%, 1.59 g/cm^3 and 1.81 g/cm^3, 9.82% and 11.57%, respectively. The P, D, and WAR of the reference sample were 21.00%, 1.62 g/cm^3, and 11.23%, respectively. The test results revealed that ES incorporation of up to 30% gradually decreased the P of the mortar. As expected from the decrease in P of the mortar, which became more compact, the D gradually increased, whereas its WAR decreased. These changes detected in physical properties were also compatible with mechanical test results. The improvement detected in the physical properties might also originate from the coexistence of NASH and CASH gels simultaneously in the AAM matrix, which enabled more voids to be filled with reaction products.

Furthermore, the micro-aggregate effect of ES particles might result in a decrease in the pore ratio of the AAM matrix. The highest D (1.81 g/cm^3) and the lowest P and WAR (15.35% and 9.82%, respectively) were detected in the samples with 70% of MK and 30% of ES contents. Beyond this optimum ratio, the physical properties of the samples deteriorated rapidly. This decreasing trend might be because alkaline activation reactions could not develop sufficiently in the ES-rich mortars with insufficient silica and alumina ratios.

The DS of AAMs is a significant property. As AAM solidifies, the free water within the pores migrates to the surface and subsequently evaporates. The evaporation of this water over time results in hydrostatic tension inside the capillary pores of the matrix, which subsequently causes the formation of microcracks in the matrix. Because aggressive chemicals could inevitably infiltrate through cracks, the infiltration shortens the material's service life (durability) [44]. Figure 7 shows the DS behaviour of the AAM samples over time.

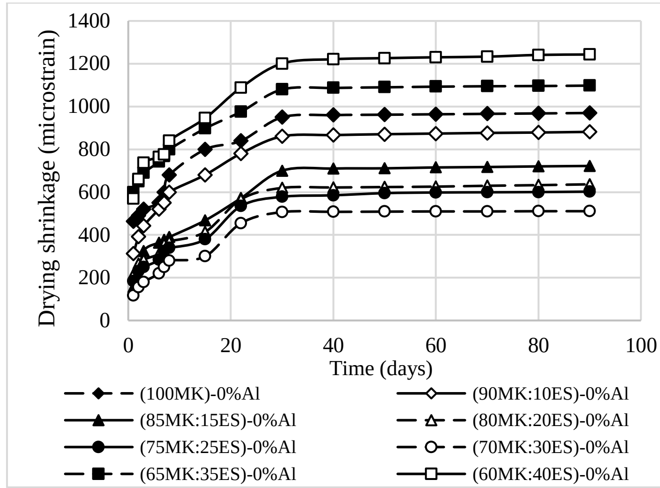

Fig. 7 The drying shrinkages of the AAM as a function of the 90-day curing period at ambient conditions

The samples experienced rapid drying during the initial curing period. The DS curves of all the samples had a high slope until day 21. However, the curves had a horizontal trend from the 21st day to the 90th day. The DS of the reference sample without ES was 970 microstrain after 90 days. The substitution of MK with ES at 10%, 15%, 20%, 25%, and 30% decreased the DS of the samples by 9%, 25%, 34%, 37%, and 47% after 90 days, respectively. The decreasing trend of DS was due to ES particles restricting DS through their micro-aggregate effect within the AAM matrix. However, ES incorporation beyond 30% adversely influenced the DS values. 35% and 40% ES inclusion led to an increase in DS by 13% and 28%, respectively, compared to the reference mixture. The highest DS (1242 microstrain) was determined in the (60MK:40ES)-0%Al sample. AAMs, especially with 35% and 40% ES contents, had high P and low D. This high P allowed water to evaporate faster from the matrix, leading to increased capillary forces in the matrix and consequently resulting in high DS values. Such results concurred with earlier findings [25, 42, 45].

Typical DS values are 816 microstrain for OPC-based mortars and 1000-2500 microstrain for normal-weight AAMs [46] after 28 days. OPC-based mortars showed 987 microstrain DS after 90 days [46]. The lowest DS value of 511 microstrains, which was obtained from 70MK:30ES samples, was remarkably lower than the OPC-based mortars as well as normal-weight AAMs.

Correlation between the 28-day CS and DS of the AAM samples is given in Figure 8. This linear correlation for the samples was Equation (10):

$$DS = -222.43 \times CS + 3231.1 \quad (10)$$

The high correlation factor of 0.9603 indicated a strong linear relationship between CS and DS of the MK- and ES-based one-part AAMs. The high CS values detected in the samples with low DS could be explained by the fact that the samples had a more compact internal structure with low P.

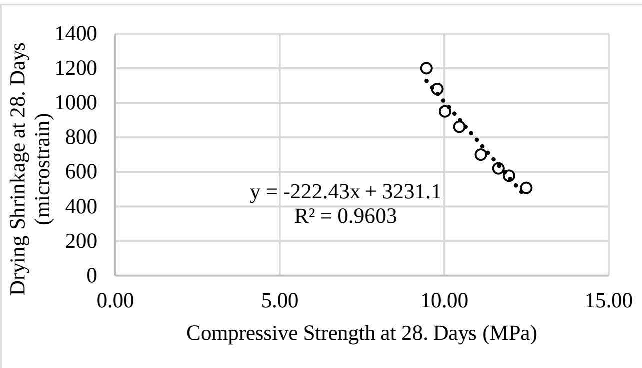

Fig. 8 Correlation between 28-day compressive strength and drying shrinkage of the AAM

3.3. The Impact of Al Content on the Mechanical Properties of the AAFM

The effects of the Al content on the mechanical properties of the 70MK:30ES AAFM samples are present in Figure 9. The UV and CS values of the (70MK:30ES)-0%Al sample were 2.33 km/s and 12.50 MPa, respectively. The significant decrease in UV and CS observed in the samples with 0.25% Al was due to Al reacting with NaOH in an aqueous environment, which released H_2 gas according to Equation (1). During the reactions, volume expansion of the AAFM occurred, and porous internal structures formed. The samples with the lowest Al content (0.25%) exhibited a UV of 1.57 km/s and a CS of 8.23 MPa. With the gradual increase in the Al content up to 1.50%, the descending trend in mechanical properties continued to decrease linearly because of forming a more porous matrix structure. This result was consistent with the findings of Kioupis et al. [47], in which porous AAFMs were produced by using Al and zinc powders. In addition, increasing the Al contents in the waste glass powder-based [12], and GGBS+FA+ES+SD-based [2] AAFMs resulted in a decrease in D and CS values.

Usually, foam-based building materials are not used for load-bearing applications. However, they must develop early strength to support the material during transportation and installation without damaging the porous structure. In the current study, 1.50% Al-containing samples, [(70MK:30ES)-1.50%Al], had 0.85 km/s UV and 4.11 MPa CS, which was adequate for the AAFM to meet the expected performance during the transportation and installation stages without damage.

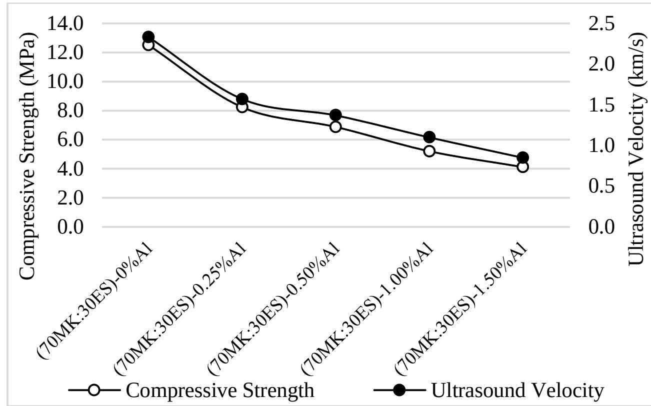

Fig. 9 The impact of Al content on the mechanical properties of AAFM

3.4. The Impact of Al Content on the Physical Properties of the AAFM

The effects of the Al content on the physical properties of the 70MK:30ES AAFM samples are present in Figure 10.

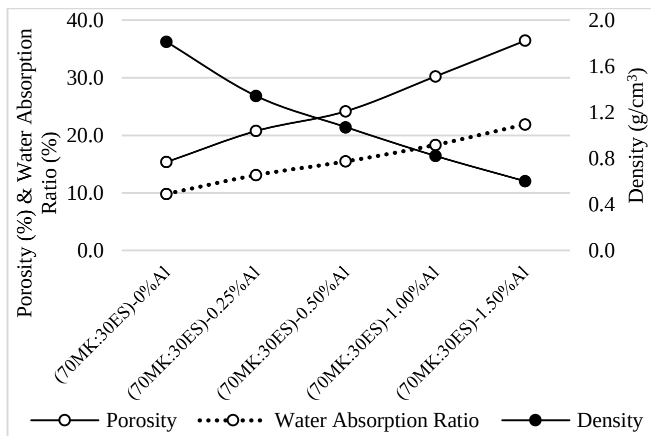

Fig. 10 The impact of Al content on the physical properties of AAFM

The P, D, and WAR of the (70MK:30ES)-0%Al sample were 15.35%, 1.81 g/cm^3, and 9.82%, respectively. The observed increase in P and WAR and decrease in D in the samples with 0.25% Al was due to the entrapped air voids in the porous internal structure of the AAFM after volume expansion. It was found that a continuous reduction in D up to 0.60 g/cm^3 depends on the increase in the Al content from 0.25% to 1.5% of the precursor. On the contrary, the P and WAR of the samples increased to 36.45% and 21.89%, respectively. In addition, there was a parallel relationship between P and WAR. The current results also correspond well with those of earlier studies. Liu et al. [1], Azarhomayun et al. [48], and Shen et al. [49] also reported that there was a positive correlation between the Al-powder content and both P and WAR and a negative impact on the mechanical properties of AAFMs. On the other hand, higher D (1.79-1.92 g/cm^3) values of GGBS+FA-based AAFMs containing 5 wt.% of SD and 10 wt.% of ES (foamed with 0.3-1.50% Al) in the literature [2] may be attributed to the type of the aluminosilicate source with higher calcium content, leading to the development of CASH gel along with NASH gel, leading to the formation of a more compact matrix structure.

The pore structure significantly influences the performance of AAFMs. The increased P significantly influences the properties of AAFMs, including permeability, strength, and TC, which are closely associated with the pore structure. The pore types of AAFMs may be divided into four groups: macropores (intentionally generated air bubbles) with size larger than 10 µm (level-1); meso pores between 0.1 µm and 10 µm, which consist of cracks inside or surrounding the unreacted particles (level-2); nanopores with size between 0.002 µm and 0.1 µm, which consist of gel interstices in the matrix (level-3); molecular pores with a size smaller than 0.002 µm, which consist of interstices in the aluminosilicate networks (level-4) [50]. Figures 11 and 12 illustrate the impact of the Al content on the pore size distributions and volume fraction of AAFMs. Table 2 shows the samples' individual and total pore volumes calculated from MIP data.

In samples without Al, the volume of nanopores, composed of gel interstices in the AAFM matrix (level-3), constituted 88.53% of the total pores (0.355 mL/g) and was more prevalent in the internal structure compared to other types of pores. In addition, the volume of these pores in the same sample was approximately 1.26-3.22 times higher than in other Al-containing samples.

The higher the volume of these nanopores, the better the development of NASH gel, therefore enhancing the mechanical properties of the material. However, the incorporation of Al in the mixture caused an increase in the volume of larger pores. 0.25% Al-containing samples had 70.16% of nanopores (level-3= 0.301 mL/g), 11.19% of micropores (level-2= 0.048 mL/g) and 18.65% of macropores with a size larger than 10 µm (level-1= 0.08 mL/g).

Gradually increasing Al content up to 1.50% resulted in an increase in the volume of macropores. 1.50% Al-containing samples had the lowest volume of nanopores (27.44%, 0.267 mL/g) and the highest volume of macropores (45.73%, 0.445 mL/g) compared to other samples. The increase in the macropore content in samples containing more foaming agents also agrees with the findings of previous research conducted by Abdellatief et al. [2].

As shown in Table 2, for AAFMs with 0.25, 0.50, 1.00 and 1.50% Al contents, the total pore volumes were 0.429 mL/g, 0.693 mL/g, 0.831 mL/g, and 0.973 mL/g, which were 1.07, 1.73, 2.07, and 2.42 times higher than the reference sample. The higher the Al content, the higher the total pore volumes in AAFMs. This result also conformed with the results of P, as explained above.

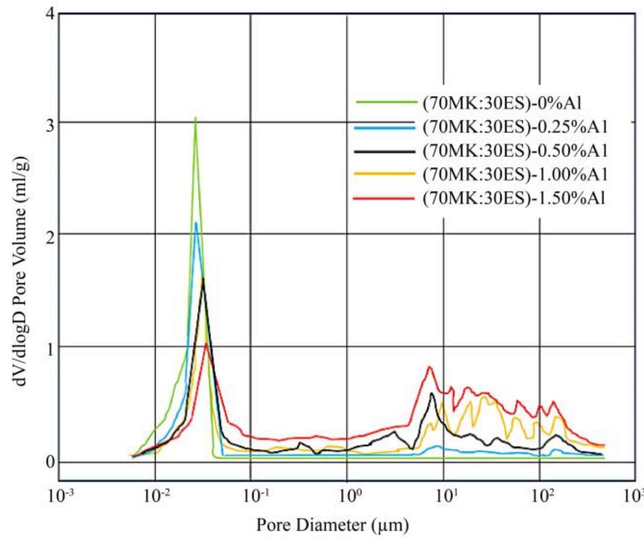

Fig. 11 The impact of Al content on the pore size distribution of AAFM

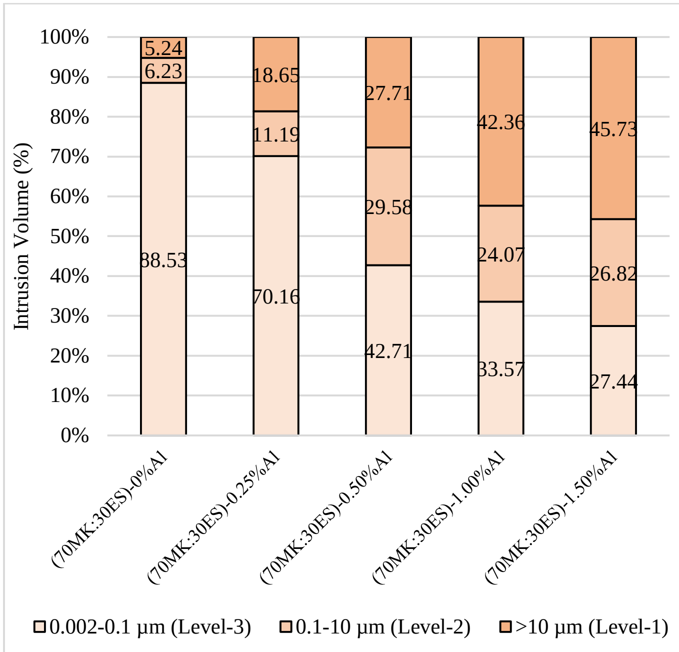

Fig. 12 The impact of Al content on the pore volume fraction of AAFM

Table 2. Pore volumes of AAFM obtained from the MIP test

Sample	Pore Volume (mL/g)			Total (mL/g)
	Level-3	Level-2	Level-1	
(70MK:30ES)-0%Al	0.355	0.025	0.021	0.401
(70MK:30ES)-0.25%Al	0.301	0.048	0.080	0.429
(70MK:30ES)-0.50%Al	0.296	0.205	0.192	0.693
(70MK:30ES)-1.00%Al	0.279	0.200	0.352	0.831
(70MK:30ES)-1.50%Al	0.267	0.261	0.445	0.973

3.5. The Impact of Al Content on the Thermal Properties of the AAFM

The effects of the Al content on the TC of the 70MK:30ES samples are present in Figure 13(a). In addition, the correlation between TC and D of the samples is given in Figure 13(b).

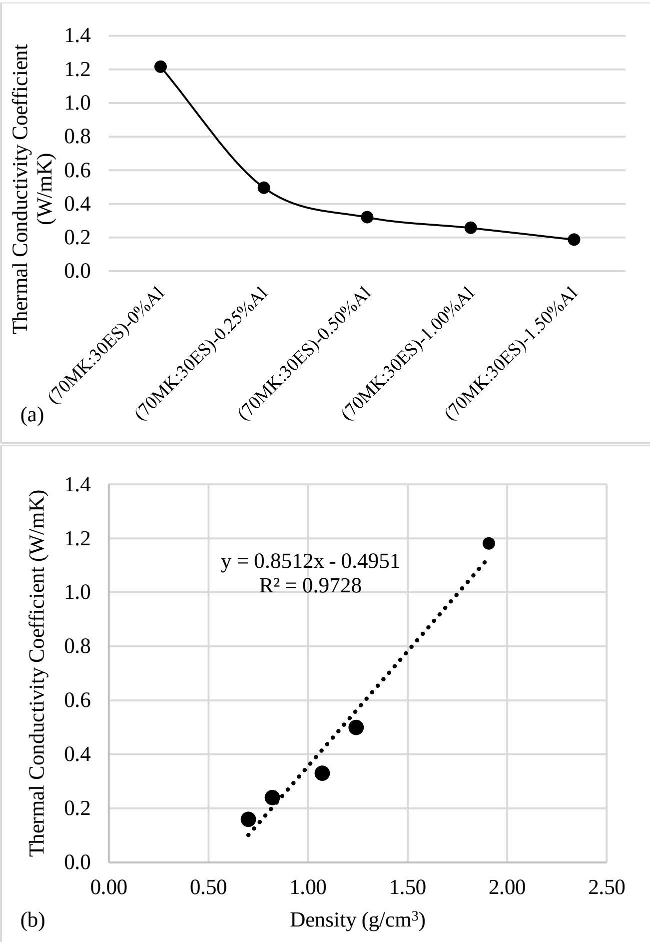

Fig. 13(a) The impact of Al content on the thermal conductivity coefficient of AAFM, (b) The correlation between thermal conductivity coefficient and density of the samples

The TC of the (70MK:30ES)-0%Al sample was 1.215 W/mK. The incorporation of Al and the gradual increase of Al content up to 1.50% resulted in a decrease in the TC of the AAFMs. This occurred as a result of the foaming agent (Al) creating many closed pores in the AAM matrix. Since the TC of still-air within these closed pores (0.026 W/mK) is significantly lower than that of the solid AAM matrix (1.215 W/mK), the porous structure within the AAFM serves as thermal insulation. It might be inferred that there was a negative correlation between P and TC in AAFMs. The lowest TC (0.187 W/mK) was found in the sample coded (70MK:30ES)-1.50%Al, which had the highest P. It was suggested that AAFMs with different thermal insulation properties could be achieved by modifying the Al content. According to regression analysis, there was also a strong linear relationship between the TC and D of AAFMs (R^2 = 0.9728), as shown in Figure 13(b).

The D, TC, and CS values of AAFMs are compared with those of various conventional materials commonly used in the building sector (Table 3). In line with this comparison, (70MK:30ES)-0%Al and (70MK:30ES)-0.25%Al samples may fulfil the D, TC and CS requirements of lightweight aggregate concrete and sand-lime bricks.

The (70MK:30ES)-0.50%Al sample has also succeeded in meeting the standard requirements for pumice concrete. (70MK:30ES)-1.00%Al sample meets the limit values of pumice concrete, aerated autoclaved concrete, and vertically perforated lightweight bricks. (70MK:30ES)-1.50%Al sample can fulfil the requirements of pumice concrete and aerated autoclaved concrete. In that case, one part AAFMs with various Al contents may be used as a non-loadbearing wall material.

The D, TC, and CS of AFFMs are compared with those of AAFMs having different raw materials (Table 4). The lowest TC of this study (0.187 W/mK) is higher than that of FA-based H_2O_2-containing foam [5], FA-based Al-containing foam [6], and MK and SD-based H_2O_2-containing foam [11]. The D and CS results of these studies [5-6, 11] are lower and higher than those of the current study, respectively.

This means that FA- and MK+SD-based aluminosilicate raw materials enable the formation of a more porous matrix. On the other hand, the TC, D and CS values of the MK+ES-based AFFMs are similar to those of MK+BA-based [3], MK-based [9], red mud+slag-based [13], and MK+FA-based [52] H_2O_2-containing foams, as well as MK-based SF-containing foam [8].

Regardless of whether H_2O_2 or Al is utilized as the foaming agent, the results containing MK are closer to each other, and the values obtained in this study compared to the results containing FA. That is, the change in the properties of the samples may be due more to the different types of aluminosilicate sources than to the type of foaming agent. However, the higher D, TC and CS values of GGBS+FA+ES+SD-based Al-containing foams [2] can be attributed to the aluminosilicate mixture having a composition with a higher calcium content, leading to the development of CASH gel as well as NASH gel.

This results in the matrix voids filling with more alkali activation reaction products and developing a better internal structure. However, the differences in the results obtained under different production and curing conditions applied during the experimental research process should also be considered.

Table 3. Comparison of AAFM properties with other conventional building materials

Material	Density (g/cm^3)	Thermal conduc. (W/mK)	Compressive strength (MPa)
Conventional concrete [51]	2.20	1.65	16.00-30.00
Lightweight aggregate concrete [51]	0.80-2.00	0.39-1.60	>4.00
Pumice-based concrete [51]	0.40-1.30	0.11-0.46	2.50-7.50
AAC-based concrete [51]	0.40-1.00	0.10-0.30	>4.00
Clay-based perforated brick (vertical) [51]	0.55-1.00	0.21-0.28	2.50-7.50
Clay-based perforated brick (horizontal) [51]	0.60-1.00	0.33-0.45	2.50-5.00
Sand-lime brick [51]	0.70-2.20	0.35-1.30	5.00-25.00
(70MK:30ES)-0%Al	**1.81**	**1.215**	**12.50**
(70MK:30ES)-0.25%Al	**1.34**	**0.496**	**8.23**
(70MK:30ES)-0.50%Al	**1.07**	**0.320**	**6.87**
(70MK:30ES)-1.00%Al	**0.82**	**0.257**	**5.20**
(70MK:30ES)-1.50%Al	**0.60**	**0.187**	**4.11**

Table 4. Comparison of AAFM properties with other alkali-activated foams produced with various aluminosilicate precursors and foaming agents

Reference	Raw material	Foaming agent	Density (g/cm^3)	Thermal conduc. (W/mK)	Compressive strength (MPa)
[2]	GGBS+FA+ES+SD	0.3-1.50% Al	1.79-1.92	1.167-1.237	9.37-17.45
[3]	MK+BA	0.5-1.5% H_2O_2	0.64-1.27	0.15-0.45	2.0-15
[5]	FA	0.05-0.1% H_2O_2	0.24-0.37	0.07-0.09	0.4-1.4
[6]	FA	0.16% H_2O_2	0.31-0.97	0.083-0.184	-
		0.16% Al	0.50-0.77	0.099-0.159	-
[7]	GGBS+FA	1.34% SP	0.64-0.82	0.27-0.32	4.2-4.8
[8]	MK	SF	0.30-0.85	0.12-0.33	-
[9]	MK	11.0% H_2O_2	0.35-1.20	0.13-0.32	0.4-5.65
[11]	MK+SD	0.03-0.24% H_2O_2	0.20-1.0	0.112-0.125	0.76-1.71
[12]	Waste glass powder	2.0-20.0% Al	0.23-0.55	0.065-0.186	3.0-8.1
[13]	Red mud+slag	1.0-5.0% H_2O_2	0.57-1.28	0.169-0.435	1.20-18.15
[52]	MK+FA	0.03-1.20% H_2O_2	0.56-1.20	0.10-0.44	2.0-9.0
This study	**MK+ES**	**0.25-1.50% Al**	**0.60-1.34**	**0.187-0.496**	**4.11-8.23**
BA:Bagasse ash, SD:sawdust, SF: Silica fume, SP: Sodium perborate					

4. Conclusion

The current study concludes with the following points:

- ES waste can be an alternative aluminosilicate source to produce one-part AAFM with adequate physical, mechanical, and thermal properties for use in the building industry as non-loadbearing wall material.
- MK:ES and Al contents are key parameters in the evolution of the material properties.
- ES substituted at 30% of MK decreased the P and WAR and increased the D, UV, and CS of AAM. The incorporation of ES provided a more compact and denser microstructure and increased the material's properties due to the development of CASH gel alongside NASH because of the high CaO concentration of ES. In addition, the unreacted ES components, consisting of $CaCO_3$, acted as micro-aggregates, and this micro-aggregate effect of ES particles enabled an increase in the properties.
- The highest D (1.81 g/cm^3), UV (2.33 km/s), CD (12.50 MPa) and the lowest P (15.35%), WAR (9.82%), and DS (511 µs) were detected in the samples with 70% of MK and 30% of ES contents.
- The Al content (up to 1.50%) and the P and WAR are positively correlated. However, there is an adverse effect on the mechanical characteristics of AAFMs. However, the mechanical properties were adequate for the AAFM to meet the expected performance during the transportation and installation of the material without damaging its porous structure.
- The pore types and pore size distributions of AAFM were changed by changes in Al content. Gradually increasing Al content up to 1.50% resulted in an increase in the volume of macropores. In addition, the higher the Al content, the higher the total pore volumes in AAFMs.
- The formation of many closed macropores in AAFM by increasing Al content up to 1.50% resulted in a decrease in TC, indicating a higher thermal insulation capacity of the AAFM. The lowest TC was 0.187 W/mK, determined

in the (70MK:30ES)-1.50%Al sample.

- MK and ES-based one-part AAFMs with various Al contents may be used as non-loadbearing wall materials similar to those commonly used in the building sector, such as lightweight aggregate concrete, pumice concrete, aerated autoclaved concrete, vertically perforated lightweight bricks, and sand-lime bricks. However, the durability characteristics of AAFMs, such as wetting-drying, freezing-thawing, and high temperatures, should be identified by applying detailed experimental methods. Furthermore, future research should conduct economic evaluations to provide practical options for industrial-scale applications.

Acknowledgments

The author would like to thank Balmumcu Chemical Company for providing the alkaline activators and Ytong Industry for providing finely ground silica sand and aluminium powder to produce one-part alkali-activated foam mortar.

References

[1] Yun-Lin Liu et al., "Foaming Processes and Properties of Geopolymer Foam Concrete: Effect of the Activator," *Construction and Building Materials*, vol. 391, 2023. [CrossRef] [Google Scholar] [Publisher Link]

[2] Mohamed Abdellatief et al., "Physico-Mechanical, Thermal Insulation Properties, and Microstructure of Geopolymer Foam Concrete Containing Sawdust Ash and Egg Shell," *Journal of Building Engineering*, vol. 90, 2024. [CrossRef] [Google Scholar] [Publisher Link]

[3] Thammaros Pantongsuk et al., "Effect of Hydrogen Peroxide and Bagasse Ash Additions on Thermal Conductivity and Thermal Resistance of Geopolymer Foams," *Materials Today Communications*, vol. 26, 2021. [CrossRef] [Google Scholar] [Publisher Link]

[4] Peter Duxson et al., "The Role of Inorganic Polymer Technology in the Development of 'Green Concrete'," *Cement and Concrete Research*, vol. 37, no. 12, pp. 1590-1597, 2007. [CrossRef] [Google Scholar] [Publisher Link]

[5] Junjie Feng et al., "Development of Porous Fly Ash-Based Geopolymer with Low Thermal Conductivity," *Materials & Design (1980-2015)*, vol. 65, pp. 529-533, 2015. [CrossRef] [Google Scholar] [Publisher Link]

[6] Michał Łach et al., "Determination of the Influence of Hydraulic Additives on the Foaming Process and Stability of the Produced Geopolymer Foams," *Materials*, vol. 14, no. 17, pp. 1-14, 2021. [CrossRef] [Google Scholar] [Publisher Link]

[7] Viengsai Phavongkham et al., "Effects of Surfactant on Thermo-Mechanical Behavior of Geopolymer Foam Paste Made with Sodium Perborate Foaming Agent," *Construction and Building Materials*, vol. 243, 2020. [CrossRef] [Google Scholar] [Publisher Link]

[8] Joseph Henon et al., "Potassium Geopolymer Foams Made with Silica Fume Pore Forming Agent for Thermal Insulation," *Journal of Porous Materials*, vol. 20, pp. 37-46, 2013. [CrossRef] [Google Scholar] [Publisher Link]

[9] Yingjie Qiao et al., "Effects of Surfactants/Stabilizing Agents on The Micro-Structure and Properties of Porous Geopolymers by Direct Foaming," *Journal of Asian Ceramic Societies*, vol. 9, no. 1, pp. 412-423, 2021. [CrossRef] [Google Scholar] [Publisher Link]

[10] E. Kamseu et al., "Bulk Composition and Microstructure Dependence of Effective Thermal Conductivity of Porous Inorganic Polymer Cements," *Journal of European Ceramic Society*, vol. 32, no. 8, pp. 1593-1603, 2012. [CrossRef] [Google Scholar] [Publisher Link]

[11] Si Zou et al., "Experimental Research on an Innovative Sawdust Biomass-Based Insulation Material for Buildings," *Journal of Cleaner Production*, vol. 260, 2020. [CrossRef] [Google Scholar] [Publisher Link]

[12] Dilan Polat, and Mustafa Güden, "Processing and Characterization of Geopolymer and Sintered Geopolymer Foams of Waste Glass Powders," *Construction and Building Materials*, vol. 300, 2021. [CrossRef] [Google Scholar] [Publisher Link]

[13] Shu Yan et al., "Microstructure Evolution and Properties of Red Mud/Slag-Based Cenosphere/Geopolymer Foam Exposed to High Temperatures," *Ceramics International*, vol. 49, no. 22, pp. 34362-34374, 2023. [CrossRef] [Google Scholar] [Publisher Link]

[14] Review of Global Egg Production 2023, Compassion in Food Business, pp. 1-6, 2023. [Online]. Available: https://www.compassioninfoodbusiness.com/resources/laying-hens/review-of-global-egg-production-2023/

[15] A. Travel, Y. Nys, and M. Bain, *Effect of Hen Age, Moult, Laying Environment and Egg Storage on Egg Quality*, Improving the Safety and Quality of Eggs and Egg Products, Woodhead Publishing, pp. 300-329, 2011. [CrossRef] [Google Scholar] [Publisher Link]

[16] Navaratnarajah Sathiparan, "Utilization Prospects of Eggshell Powder in Sustainable Construction Material – A Review," *Construction and Building Materials*, vol. 293, 2021. [CrossRef] [Google Scholar] [Publisher Link]

[17] Navdeep Singh, and S.P. Singh, "Validation of Carbonation Behavior of Self Compacting Concrete Made with Recycled Aggregates Using Microstructural and Crystallization Investigations," *European Journal of Environmental and Civil Engineering*, vol. 24, no. 13, pp. 2187-2210, 2020. [CrossRef] [Google Scholar] [Publisher Link]

[18] Poonam Shekhawat, Gunwant Sharma, and Rao Martand Singh, "Strength Behavior of Alkaline Activated Eggshell Powder and Fly Ash Geopolymer Cured at Ambient Temperature," *Construction and Building Materials*, vol. 223, pp. 1112-1122, 2019. [CrossRef] [Google Scholar] [Publisher Link]

[19] Vijayvenkatesh Chandrasekaran et al., "Experimental Investigation of Partial Replacement of Cement with Glass Powder and Eggshell Powder Ash in Concrete," *Civil Engineering Research Journal*, vol. 5, no. 3, 2018. [CrossRef] [Google Scholar] [Publisher Link]

[20] Ashfaque Ahmed Jhatial et al., "Green and Sustainable Concrete – The Potential Utilization of Rice Husk Ash and Egg Shells," *Civil Engineering Journal*, vol. 5, no. 1, pp. 74-81, 2019. [CrossRef] [Google Scholar] [Publisher Link]

[21] P. Shekhawat, G. Sharma, and R. M. Singh, "Microstructural and Morphological Development of Eggshell Powder and Flyash-Based Geopolymers," *Construction and Building Materials*, vol. 260, 2020. [CrossRef] [Google Scholar] [Publisher Link]

[22] Poonam Shekhawat, Gunwant Sharma, and Rao Martand Singh, "Morphology and Microstructure of Waste Material-Based Geopolymer with Flyash, Eggshell Powder, and Soft Soil," *Materials Letters*, vol. 334, 2023. [CrossRef] [Google Scholar] [Publisher Link]

[23] Arulanantham Anburuvel et al., "Characteristic Evaluation of Geopolymer Based Lateritic Soil Stabilization Enriched with Eggshell Ash and Rice Husk Ash for Road Construction: An Experimental Investigation," *Construction and Building Materials*, vol. 387, 2023. [CrossRef] [Google Scholar] [Publisher Link]

[24] M.O.M. Mashri et al., "Enhancing the Properties of UPOFA-Based Geopolymer Mortar via the Incorporation of Eggshell Ash and Silica Fume," *Journal of Building Engineering*, vol. 65, 2023. [CrossRef] [Google Scholar] [Publisher Link]

[25] Tarik Omur, Nausad Miyan, and Nihat Kabay, "Utilization of Eggshell Powder in One-Part Alkali-Activated Metakaolin Based Binder," *Construction and Building Materials*, vol. 445, 2024. [CrossRef] [Google Scholar] [Publisher Link]

[26] Xiongzhou Yuan et al., "Evaluation of The Performance of High- Strength Geopolymer Concrete Prepared with Recycled Coarse Aggregate Containing Eggshell Powder and Rice Husk Ash Cured at Different Curing Regimes," *Construction and Building Materials*, vol. 434, 2024. [CrossRef] [Google Scholar] [Publisher Link]

[27] Isabel Pol Segura et al., "Comparison of One-Part and Two-Part Alkali-Activated Metakaolin and Blast Furnace Slag," *Journal of Sustainable Metallurgy*, vol. 8, pp. 1816-1830, 2022. [CrossRef] [Google Scholar] [Publisher Link]

[28] Jie Ren et al., "Experimental Comparisons between One-Part and Normal (Two-Part) Alkali-Activated Slag Binders," *Construction and Building Materials*, vol. 309, 2021. [CrossRef] [Google Scholar] [Publisher Link]

[29] TS25, Data Sheet, Alldatasheet.Net. [Online]. Available: https://www.alldatasheet.net/view_datasheet.jsp?sSearchword=TS25&aPage=11&sField=3

[30] M.N. Freire, and J.N.F. Holanda, "Characterization of Avian Eggshell Waste Aiming Its Use in A Ceramic Wall Tile Paste," *Cerâmica*, vol. 52, pp. 240-244, 2006. [CrossRef] [Google Scholar] [Publisher Link]

[31] Ailar Hajimohammadi, Tuan Ngo, and Priyan Mendis, "How Does Aluminium Foaming Agent Impact The Geopolymer Formation Mechanism?," *Cement and Concrete Composites*, vol. 80, pp. 277-286, 2017. [CrossRef] [Google Scholar] [Publisher Link]

[32] TS-EN1015-10, Turkish Standard Institution, pp. 1-5, 2001. [Online]. Available: https://intweb.tse.org.tr/standard/standard/Standard.aspx?081118051115108051104119110104055047105102120088111043113104073081122083086079114097110065054057/

[33] TS-EN13755, Turkish Standard Institution, pp. 1-10, 2009. [Online]. Available: https://intweb.tse.org.tr/Standard/Standard/Standard.aspx?081118051115108051104119110104055047105102120088111043113104073102077043081050079068102067073056/

[34] TS699, Turkish Standard Institution, pp. 1-42, 2009. [Online]. Available: https://www.jmo.org.tr/resimler/ekler/596097c2f3799b4_ek.pdf/

[35] TS-EN1920-8, Data Sheet, Alldatasheet.Net. [Online]. Available: https://www.alldatasheet.net/view_datasheet.jsp?Searchword=TS-EN1920-8

[36] ASTM-C518-17, ASTM International. [Online]. Available: https://intweb.tse.org.tr/Standard/Standard/Standard.aspx?081118051115108051104119110104055047105102120088111043113104073102077043081050079068102067073056/

[37] TS-EN14579, Turkish Standard Institution, pp. 1-14, 2006. [Online]. Available: https://intweb.tse.org.tr/Standard/Standard/Standard.aspx?053107106111065067115113049116090107100056052055108081090071086075069085047110067109075073081116103090081086073108065117084119099101051071084104077111067108100082105053088112067066106067118112/

[38] TS-EN196-1, Turkish Standard Institution, pp. 1-31, 2009. [Online]. Available: https://intweb.tse.org.tr/standard/standard/Standard.aspx?081118051115108051104119110104055047105102120088111043113104073088066113082087078107067083069056/

[39] Alessandro Filipponi, Giulia Masi, and Maria Chiara Bignozzi, "Pressing Metakaolin-Based One-Part Geopolymers: Influence of the Mix Design on Microstructural and Physical Properties," *Ceramics International*, vol. 48, no. 4, pp. 5814-5823, 2022. [CrossRef] [Google Scholar] [Publisher Link]

[40] Kang-Wei Lo et al., "Synthesis Metakaolin-Based Geopolymer Incorporated with SIC Sludge using Design of Experiment Method," *Polymers*, vol. 14, no. 16, pp. 1-13, 2022. [CrossRef] [Google Scholar] [Publisher Link]

[41] C.K. Yip et al., "The Coexistence of Geopolymeric Gel and Calcium Silicate Hydrate at the Early Stage of Alkaline Activation," *Cement and Concrete Research*, vol. 35, no. 9, pp. 1688-1697, 2005. [CrossRef] [Google Scholar] [Publisher Link]

[42] Christina K. Yip et al., "Carbonate Mineral Addition to Metakaolin-Based Geopolymers," *Cement and Concrete Composites*, vol. 30, no. 10, pp. 979-985, 2008. [CrossRef] [Google Scholar] [Publisher Link]
[43] Deluan Feng et al., "Experimental Study on Preparation of Fly Ash-Based Geopolymer Blended with Recycled Calcium Source," *Sustainable Materials and Technologies*, vol. 41, 2024. [CrossRef] [Google Scholar] [Publisher Link]
[44] Ailar Hajimohammadi, Tuan Ngo, and Alireza Kashani, "Sustainable One-Part Geopolymer Foams with Glass Fines Versus Sand as Aggregates," *Construction and Building Materials*, vol. 171, pp. 223-231, 2018. [CrossRef] [Google Scholar] [Publisher Link]
[45] Adem Ahıskalı et al., "Mechanical and Durability Properties of Polymer Fiber Reinforced One-Part Foam Geopolymer Concrete: A Sustainable Strategy for The Recycling of Waste Steel Slag Aggregate and Fly Ash," *Construction and Building Materials*, vol. 440, 2024. [CrossRef] [Google Scholar] [Publisher Link]
[46] P. Chindaprasirt, S. Homwuttiwong, and V. Sirivivatnanon, "Influence of Fly Ash Fineness on Strength, Drying Shrinkage and Sulfate Resistance of Blended Cement Mortar," *Cement and Concrete Research*, vol. 34, no. 7, pp. 1087-1092, 2004. [CrossRef] [Google Scholar] [Publisher Link]
[47] D. Kioupis et al., "Development of Porous Geopolymers Foamed by Aluminum and Zinc Powders," *Ceramics International*, vol. 47, no. 18, pp. 26280-26292, 2021. [CrossRef] [Google Scholar] [Publisher Link]
[48] Fazel Azarhomayun et al., "Effect of Calcium Stearate and Aluminum Powder on Free and Restrained Drying Shrinkage, Crack Characteristic and Mechanical Properties of Concrete," *Cement and Concrete Composites*, vol. 125, pp. 1-12, 2022. [CrossRef] [Google Scholar] [Publisher Link]
[49] Shengwei Shen et al., "Synthesis of Industrial Solid Wastes Based Geopolymer Foams for Building Energy Conservation: Effects of Metallic Aluminium and Reclaimed Materials," *Construction and Building Materials*, vol. 328, 2022. [CrossRef] [Google Scholar] [Publisher Link]
[50] Shikun Chen et al., "Pore Structure of Geopolymer Materials and Its Correlations to Engineering Properties: A Review," *Construction and Building Materials*, vol. 328, 2022. [CrossRef] [Google Scholar] [Publisher Link]
[51] TS825, Data Sheet, Alldatasheet.Net. [Online]. Available: https://www.alldatasheet.net/view_datasheet.jsp?Searchword=TS825
[52] Rui M. Novais et al., "Porous Biomass Fly Ash-Based Geopolymers with Tailored Thermal Conductivity," *Journal of Cleaner Production*, vol. 119, pp. 99-107, 2016. [CrossRef] [Google Scholar] [Publisher Link]